physica status solidi rrl
www.pss-rapid.com

Itinerant Semiconducting Antiferromagnetism in Metastable V_3Ga

Bin He, Zhidi Bao, Kun Zhu, Wuwei Feng, Hua Sun, Ning Pang, Namsrai Tsogbadrakh, and Dorj Odkhuu**

Herein, a metastable phase of β-W type V_3Ga is identified to exhibit an itinerant semiconducting antiferromagnetism. Density functional theory plus Hubbard U (DFT+U) calculations predict the β-W type structure as a possible metastable phase, although energetically less favorable than the previously known $D0_3$ phase, which is successfully synthesized with good crystallinity by alternating evaporation method with postannealing process rather than traditional coevaporation method. Such a metastable β-W phase results in an antiferromagnetic (AFM) order up to at least 500 K and highly conductive semiconducting behavior. The antiferromagnetism in the β-W type V_3Ga can be understood in terms of strong Coulomb repulsion and Hund's rule coupling between the nearest neighbor V 3d orbital states and their covalent bonding with the Ga 4p orbitals. These results are further verified by an exchange bias phenomenon revealed in antiferro/ferromagnet hybrid heterostructure of V_3Ga and Fe films, where the strong hybridization between Fe 3d and V 3d orbital states at the interface gives rise to the robust perpendicular magnetic anisotropy therein. Herein, a novel route is used to prepare an AFM semiconductor material for antiferromagnet spintronics.

1. Introduction

Traditional spintronics rely on the control of magnetic moments of ferromagnetic (FM) materials for data storage and manipulation.[1] With the further development of information storage memory devices toward ultrafast speed, higher density capacity, and lower power consumption, the shortcomings on FM materials have been gradually revealed. Recently, an alternative concept that is based on the utilization of antiferromagnetic (AFM) materials as a key element has been proposed.[2–4] In contrast to the FM materials, the AFM materials do not produce leakage magnetic field and are not disturbed by an external magnetic field due to their zero net magnetization.[2–4] Such negligible magnetization is also indispensable to reducing the current density required for magnetization switching in magnetic tunneling junctions (MTJs).[5,6] The AFM materials can thus be integrated on a chip in higher density without suffering the interference between the magnetic moments of each unit. In addition, it is also an important advantage that the resonance frequency of AFM dynamics is 2–3 orders of magnitude higher than that in FM materials.[7–9]

Beyond these intriguing features of AFM materials, the search for an AFM with desirable physical properties, e.g., high Néel temperature, spin–orbit, anisotropic phenomena, and highly conductive semiconducting, has been very intensive. The mostly explored AFM materials thus far in this regard are Mn-based alloys, such as CuMnAs[10,11] and Mn_2Au,[12,13] and B2-ordered FeRh alloys.[2–4] The latter exhibit various intriguing physical phenomena, including a magnetic phase transition from the AFM to the FM upon heating above room temperature[14–16] and room temperature bistable AFM formation.[2,3] More recently, the FeRh thin films have been identified to exhibit even rich emergent phenomena such as thermal- and electric-field controls of magnetic phase transition[4,17,18] and magnetization reversal at the AFM–FM transition.[6,19] The high Néel temperature and strong spin–orbit coupling (SOC) make the former class of AFM materials ideal candidates for antiferromagnet spintronics.[10–13]

In contrast, Heusler alloys, with the chemical formula X_2YZ, where X and Y are transition metals and Z is the main group

B. He, Z. Bao, K. Zhu, Prof. W. Feng, Dr. H. Sun
School of Materials Science and Technology & Beijing Key Laboratory of Materials Utilization of Nonmetallic Minerals and Solid Wastes
China University of Geosciences
Beijing 100083, China
E-mail: wfeng@cugb.edu.cn

Z. Bao
Electrophysical Division
Beijing Research Institute of Automation for Machinery Industry Co. Ltd.
Beijing 100120, China

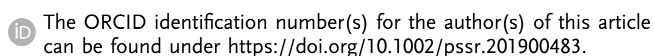
The ORCID identification number(s) for the author(s) of this article can be found under https://doi.org/10.1002/pssr.201900483.

DOI: 10.1002/pssr.201900483

Dr. N. Pang
College of Standardization
China Jiliang University
Hangzhou, Zhejiang 310018, China

Prof. N. Tsogbadrakh
Department of Physics
National University of Mongolia
Ulaanbaatar 14201, Mongolia

Prof. D. Odkhuu
Department of Physics
Incheon National University
Incheon 22012, South Korea
E-mail: odkhuu@inu.ac.kr

© 2019 WILEY-VCH Verlag GmbH & Co. KGaA, Weinheim

element, have recently drawn great attention due to their variety of magnetic properties and structural similarities to binary semiconductors.[20–24] Many of them are half-metallic or spin-gapless semiconducting magnets, which can further promote the operation of devices, owing to the spin filtering and excitation of both electrons and holes in the absence of energy gap. One type of Heusler materials is V-based V_3Z alloys crystallized in $D0_3$ structure, where now all X and Y atoms are identical.[25–27] Theoretical studies have identified that the V_3Al, V_3Ga, and V_3In alloys exhibit the G-type itinerant antiferromagnetism and gapless semiconducting characters.[27] Moreover, it was also predicted that the large AFM exchange interactions can lead to a very high Néel temperature of 878 K.[27] These predictions of the coexistence of gapless semiconducting and high Néel- temperature AFM behaviors in these compounds are of interest and can further suggest the optimization of practical synthesis and their eventual incorporation in real devices.

In this article, we report results of our experimental and first-principles calculations on an itinerant semiconducting antiferromagnetism identified in the metastable phase of β-W type V_3Ga. Our calculations first predict the β-W phase as a possible metastable phase, although energetically less favorable than $D0_3$ structure, which we have successfully grown on Si(001) substrate by electron beam evaporation in a vacuum chamber. Both experimental and theoretical studies demonstrate the AFM phase up to at least 500 K and semiconducting behavior with a narrow bandgap of 0.1–0.2 eV. Furthermore, we predict the large perpendicular magnetic anisotropy normal to the film plane in the synthetic hybrid heterostructure of V_3Ga and Fe films, as an antiferromagnet-semiconductor/ferromagnet–metal junction, which is mainly attributed to the strong hybridization between the Fe and V d-orbital states at the interface.

2. Results and Discussion

We first investigate the structural stability and magnetism of bulk V_3Ga in the $D0_3$ and β-W type A15 structures by first-principles density functional theory plus U (DFT+U) calculations. Previous DFT studies have shown that bulk V_3Ga can form in the $D0_3$ phase with the G-type AFM order.[27] Our calculations using DFT+U reproduce these results that the $D0_3$ V_3Ga favors the AFM phase in the G-type order. However, our calculations also suggest that the β-W type A15 phase cannot be ignored, which is indeed possible as a metastable phase in practical fabrication, owing to a small energy deviation (≈0.09 eV formula unit^{-1} [f.u.]) between the two phases, as shown in **Figure 1**a.

In the β-W type lattice, we have considered four different magnetic configurations to identify the most stable magnetic phase (**Figure 2**): 1) entirely FM, 2) AFM-I (spin parallel within the plane for all *ab*-, *ac*-, and *bc*-planes but antiparallel plane to plane), 3) AFM-II (spin parallel within the plane for *ac*- and *bc*-planes but antiparallel within the *ab*-plane), and 4) AFM-III (spin antiparallel within the plane for all planes). Results of the optimized lattice parameters and relative energies are shown in the table at the bottom of Figure 2 for each magnetic configuration. Notably, the β-W type V_3Ga favors the AFM-III phase in cubic lattice with $a = 4.87$ Å, which is more stable by total energy differences of 0.13, 5.65, and 5.80 eV f.u.$^{-1}$ for FM, AFM-I, and AFM-II phases, respectively. We thus refer the results and discussion here and hereafter mainly to those corresponding to the AFM-III phase, unless specifically mentioned. Apparently, such AFM phases cannot be reproduced by standard DFT calculations without the inclusion of U parameters, where the AFM phases turn out to be degenerate in energy with the spin-nonpolarized configuration (i.e., Pauli paramagnet[28]) and no net magnetism on V sites.

To validate the DFT+U results, we have prepared the $(V[0.8\,nm]/Ga[0.3\,nm])_{50}$, $(V[1.1\,nm]/Ga[0.3\,nm])_{43}$, and $(V[0.7\,nm]/Ga[0.3\,nm])_{60}$ multilayered films by the alternate evaporation (AE) method and also prepared the 60 nm-thick V–Ga films by the coevaporation (CE) method. After energy-dispersive spectrometry (EDS) composition measurement, their real proportions were $V_{3.69}Ga$ (AE), $V_{3.01}Ga$ (AE), $V_{2.29}Ga$ (AE), $V_{1.18}Ga$ (CE), and $V_{2.47}Ga$ (CE), respectively.

Figure 1b shows the θ–2θ X-ray diffraction (XRD) pattern, with a logarithmic scale being used for diffraction intensity, for V–Ga

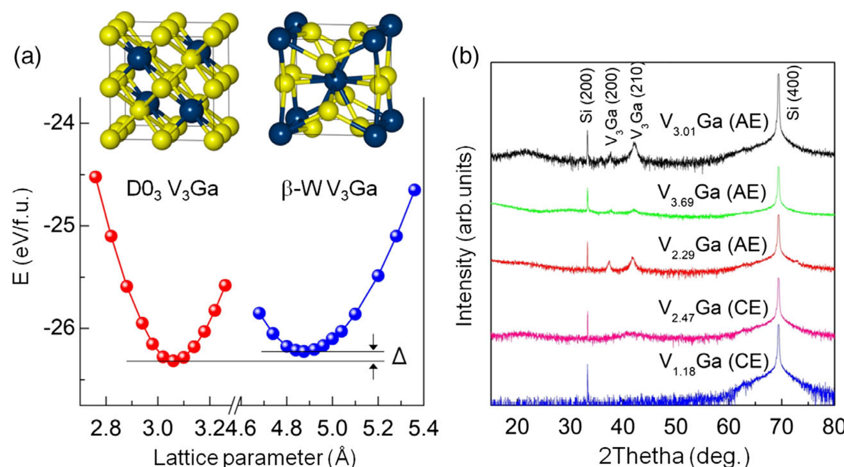

Figure 1. a) Total energies (eV f.u.$^{-1}$) of the $D0_3$ (red) and β-W type A15 (blue) phases of bulk V_3Ga as a function of the lattice parameter a (Å) from DFT+U calculations. The corresponding atomic structures are shown in the inset, where the yellow and blue spheres denote the V and Ga atoms, respectively. b) θ–2θ XRD pattern for the V–Ga films with different V concentrations.

© 2019 WILEY-VCH Verlag GmbH & Co. KGaA, Weinheim

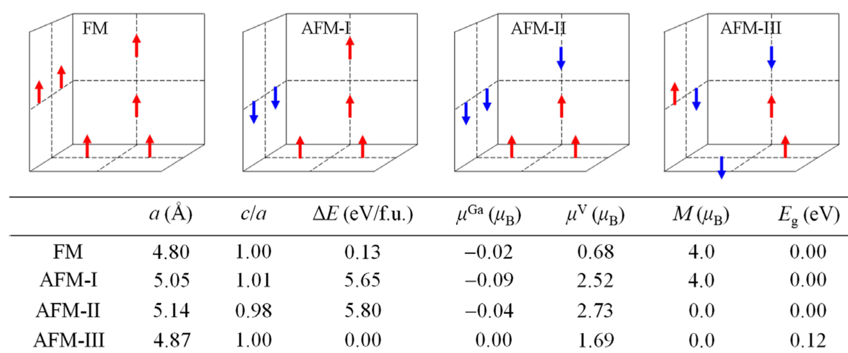

	a (Å)	c/a	ΔE (eV/f.u.)	μ^{Ga} (μ_B)	μ^{V} (μ_B)	M (μ_B)	E_g (eV)
FM	4.80	1.00	0.13	−0.02	0.68	4.0	0.00
AFM-I	5.05	1.01	5.65	−0.09	2.52	4.0	0.00
AFM-II	5.14	0.98	5.80	−0.04	2.73	0.0	0.00
AFM-III	4.87	1.00	0.00	0.00	1.69	0.0	0.12

Figure 2. Optimized lattice parameters a (Å) and c/a, relative energy ΔE (eV f.u.$^{-1}$), Ga and V-site magnetic moments μ^X and total magnetization M (μ_B), and bandgap energy E_g (eV) of the β-W type V_3Ga for the different magnetic phases, FM, AFM-I, AFM-II, and AFMIII, shown at the top. Total energy of the AFM-III phase is taken as reference energy. For simplicity, we show only three panels, *ab*-, *ac*-, and *bc*-panel, of the β-W type V_3Ga structure, where the red-upward and blue-downward arrows denote the spin orientation of V atoms.

films with different concentrations. With the exception of the diffraction peaks from the substrates, there are two resolved peaks located at the 2θ positions of 37.7 and 42.0, for the V–Ga films by the AE method, which match with the V_3Ga (200) and (210) diffractions in JCPDS 12-0086. Hence, the as-prepared crystalline V_3Ga films adopt the cubic structure with a space group of Pm3n (223), which is the β-W type A15 lattice as predicted in our computation, rather than the $D0_3$ phase. In contrast, almost no resolved peaks can be seen for the samples prepared by the CE method, and the crystallinity of the V_3Ga samples grown by the CE method is not as good as that grown by the AE method. From the analyses of field-emission scanning electron microscope (SEM) images, the stoichiometric V_3Ga sample demonstrates the most flat and homogeneous surface among the V–Ga films with different V concentrations (not shown). When Ga becomes rich ($x < 3$ in V_xGa), a local aggregation of Ga is observed, leading to the deterioration of sample homogeneity.

Figure 3a shows the magnetic hysteresis loops for V–Ga films with different concentrations, indicating that all samples exhibit the absence of FM ordering. Note that the diamagnetic signal from the Si substrate was not ruled out. In Figure 3b, the temperature-dependent magnetization variation curve shows the sign of

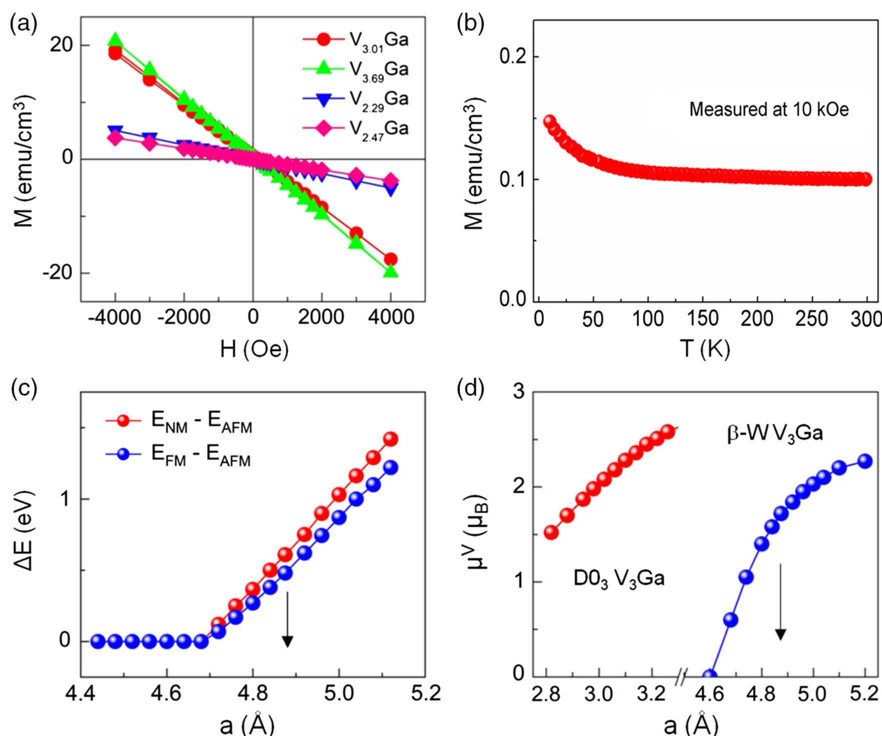

Figure 3. a) Magnetic hysteresis loops for V–Ga films with different concentrations. b) Temperature-dependent magnetization variation of $V_{3.01}Ga$ sample measured at the field of 10 kOe. DFT+U results of the c) magnetic energy and d) V-site magnetic moment of the β-W type bulk V_3Ga as a function of lattice constant a. In (d), the corresponding results in the $D0_3$ phase are also shown. The downward arrows indicate the optimized lattice parameter.

© 2019 WILEY-VCH Verlag GmbH & Co. KGaA, Weinheim

coexistence of the AFM phase and the reminiscent of paramagnetic impurities in V_3Ga films, in agreement with the observed M–T behavior of AFM Mn_2Au.[13]

As on-site Coulomb interactions play a critical role in determining antiferromagnetism, it is important to study the effects of lattice and lattice parameters on magnetism. In the most stable AFM-III phase, the magnetic energy, defined as $\Delta E = E_{NM/FM} - E_{AFM}$, and V-site magnetic moment (μ^V) versus a are shown in Figure 3c,d, respectively. At the equilibrium lattice, the antiferromagnetism is favored over the FM and nonmagnetic (NM) phases, and the magnetic moment of the V site is about $1.69\mu_B$, whereas there is no NM for the Ga site (table in Figure 2). Both the ΔE and μ^V decrease and become zero at $a \approx 4.7$ Å, which corresponds to about 3.5% reduction in lattice. In contrast, for the $D0_3$ phase, the μ^V decreases gradually and tends not to reach zero, as shown by red circles in Figure 3b. This suggests that the β-W type V_3Ga and its antiferromagnetism must be treated carefully and described as strongly covalent intermediate coupling systems like transition metal oxides (TMOs).[13]

Theories of antiferromagnetism in the β-W type V_3Ga can thus be understood in terms of strong Coulomb repulsions and Hund's rule coupling in the 3d orbitals of the transition metal V cations and their covalent bonding with the Ga $4p^1$ orbitals (Ga d^{10} orbitals are filled). Strong onsite electron interactions tend to inhibit double occupancy of the 3d orbital and the overall Coulomb energy of the crystal is lowered by localizing the valence charge of the cation. Covalent bonding delocalizes the d-electron charge and thus lowers the kinetic energy. The former mechanism favors the formation of local magnetic moments, whereas the latter decreases the moment but increases the exchange coupling between the magnetic moments of the nearest neighbor V atoms through virtual hopping processes within the plane (Figure 2).

The temperature-dependent resistance, $\rho(T)$, variation of V_3Ga films is shown in **Figure 4**a. $\rho(T)$ decreases with temperature, indicating the semiconducting nature. There is an inflection point at around 350 K. To resolve whether this corresponds to a magnetic phase transition, we analyze the applied field-dependent magnetoresistance (R–H) measurements for the different temperatures up to 500 K in Figure 4b. All the R–H curves maintain a linear feature, which clearly indicates the persistence of the AFM order up to 500 K, in line with the prediction of high Néel temperature.[20] The inset in Figure 4a shows a data fit of $\rho(T)$ above 350 K by a simple model, $\sigma(T) = \sigma_o + \sigma_a \exp(E_a/k_B T)$. The best fit yields an energy barrier (E_a) of 0.1 eV, indicating a bandgap of around 0.2 eV. Furthermore, the UV–vis spectrum measurement derives a small bandgap of around 0.16 eV (Figure 4c). The small bandgap semiconductor nature of the β-W type V_3Ga is further supported by the density of states (DOS) analyses in Figure 4d from DFT+U calculations, where the calculated bandgap (≈0.1 eV) agrees well with the measured value.

To better confirm the AFM nature of the as-prepared V_3Ga film, we further perform our experiments for 5.5 nm-thick $V_{3.01}Ga$ films on Fe(2 nm) and pure Fe(2 nm) layers on Si substrate. The magnetic layer is capped with 2 nm-thick Si layer to avoid oxidization. The magnetic and magnetoresistance hysteresis loops of the $V_{3.01}Ga$(5.5 nm)/Fe(2 nm) and Fe(2 nm) layers

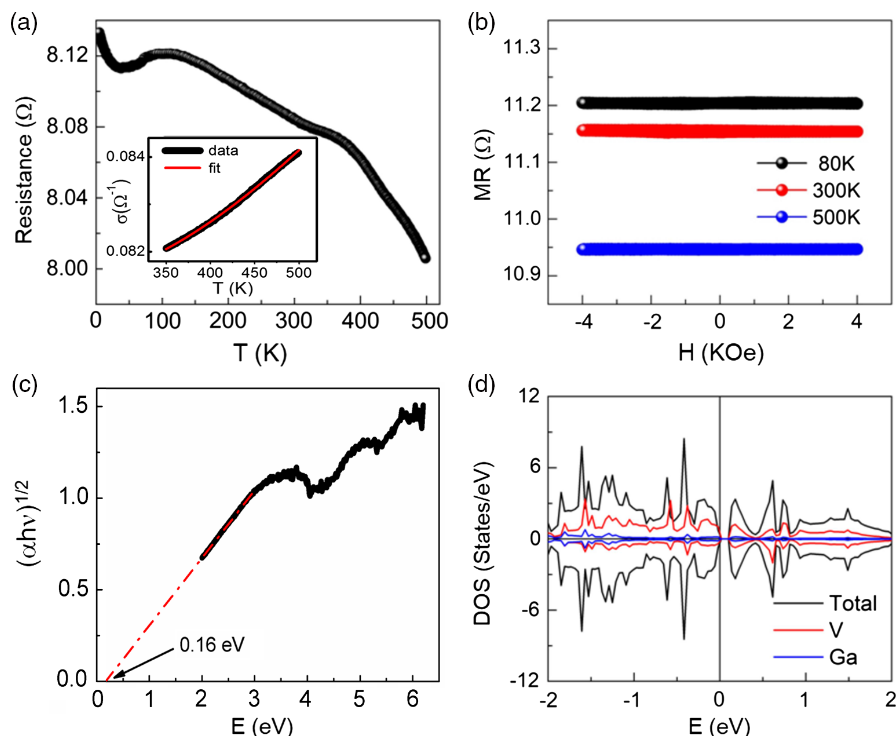

Figure 4. a) Temperature-dependent resistance, b) magnetoresistance vs applied field at different temperatures, and c) UV–vis spectrum of $V_{3.01}Ga$ sample. The inset in (a) shows a fit of $\sigma(T)$ curve above 350 K. d) Total (black line) and atom (V in red and Ga in blue)-projected DOS of the β-W type bulk V_3Ga from DFT+U calculations. The Fermi level is set to zero energy.

© 2019 WILEY-VCH Verlag GmbH & Co. KGaA, Weinheim

are shown in **Figure 5**a,b, respectively, where the room temperature magnetic hysteresis loops were measured after samples were magnetized in a field of 1.8 T for 15 min. The $V_{3.01}Ga$(5.5 nm)/Fe(2 nm) bilayer exhibits a large enhancement in coercivity compared with pure Fe(2 nm). This increase in coercivity could be caused by any one of several complications, including nanoparticles or compositional intermixing arising from annealing. We note here that Fe layer was grown on V_3Ga at room temperature to prepare the V_3Ga /Fe bilayer sample and the evaporation rate was controlled to around 0.1 $Å\,s^{-1}$ during layer deposition to guarantee the good quality of the bilayer sample. Therefore, it was believed that the enhancement of coercivity comes from the exchange anisotropy acting on Fe layers by the AFM V_3Ga layers. The exchange bias effect is further confirmed by the observation of the shifted magnetoresistance peak positions at 37.04 and 18.31 Oe, as shown in Figure 5b. As for the FM hysteresis loops, the magnetic moment of the ferromagnet tends to change direction at the field of coercivity, which is normally accompanied by the inflexion of magnetoresistance. Here at 80 K, V_3Ga /Fe bilayer shows an inflexion in the magnetoresistance, having a bias shift apparently for different directions of sweeping the field. It means that the exchange interaction between the AFM V_3Ga and FM Fe at their interface becomes more prominent at low temperatures. The exchange bias is indeed an important evidence for the presence of an AFM film.[29]

The A15 structure of bulk V_3Ga is a well-known superconductor with a transition temperature of 14 K.[30] As shown in Figure 3a, there is no superconductivity transition at the low temperature region down to 5 K. Although V_3Ga samples in our study adopt the same structure compared with A15 V_3Ga superconductor, it exhibits quite different properties. This dissimilarity is probably due to the specific film preparation procedure and the composition deviation from the stoichiometry of V_3Ga.

Finally, the interfacial local magnetism and preferable magnetization direction at the V_3Ga/Fe interface have been explored by DFT+U calculations. As shown in Figure 5c, we modeled the nine atomic layers of the β-W type V_3Ga films on five-layer-thick Fe substrate, where two different interfaces, namely V/Fe-interface (left) and VGa/Fe-interface (right), were considered. For both interfaces, the V and Ga atoms prefer the hollow adsorption site of Fe atoms at the interface. The optimized lattice constant (3.87 Å) of bulk V_3Ga was adopted for the in-plane lattice of supercells. The layer-resolved magnetization and magnetic anisotropy energy (MAE) of the V_3Ga/Fe bilayers are shown in Figure 4d. The MAE is determined from $\text{MAE} = E_{[100]} - E_{[001]}$, where the $E_{[100]}$ and $E_{[001]}$ are the total energies with magnetization along the [100] and [001] directions, respectively. For both interfaces, the AFM configuration of the β-W type V_3Ga films is almost preserved although there are small deviations in magnetism at the interface and surface regions. In particular, the magnetic moments of the interfacial V atoms are antiparallel to the interfacial Fe moments, which are slightly reduced compared with those at the center Fe layers.

As shown in Figure 5d, the MAE values within the V_3Ga layers are negligibly small. Similar phenomena can be applied to the Fe layers at the center, maintaining the high-symmetry bulk-like feature. In contrast, for both interfaces, the surface and interface Fe

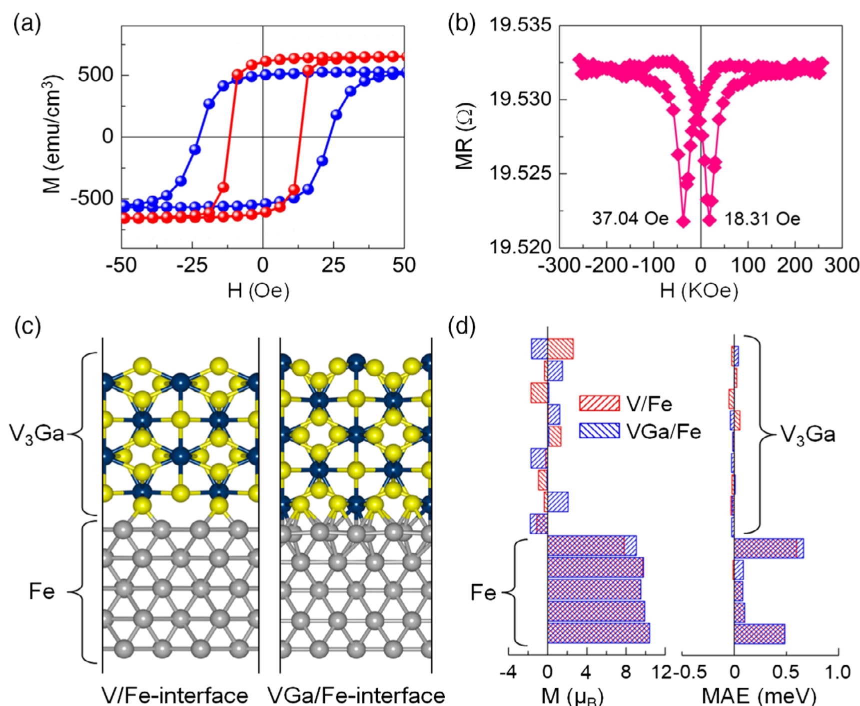

Figure 5. a) Room temperature magnetic hysteresis loops for the $V_{3.01}Ga$ (5.5 nm)/Fe (2 nm) (blue) and pure Fe (2 nm) (red) layers measured after samples were saturated in a magnetic field of 1.8 T for 15 min. b) The magnetoresistance hysteresis loop measured at 80 K for the $V_{3.01}Ga$(5.5 nm)/Fe(2 nm) bilayer. c) Side view of the optimized atomic structures of the V_3Ga /Fe bilayer with the V/Fe (left) and VGa/Fe interface (right) from DFT+U calculations. The yellow, blue, and gray spheres denote the V, Ga, and Fe atoms, respectively. d) DFT+U results of the layer-resolved magnetization (left) and MAE (right) of the V_3Ga/Fe bilayer for the V/Fe (red) and VGa/Fe interface (blue).

© 2019 WILEY-VCH Verlag GmbH & Co. KGaA, Weinheim

layers exhibit large positive MAE, owing to the anisotropic nature that mainly resides at the interface and/or surface. The positive sign in MAE stands for the preferable direction of magnetization normal to the film plane, i.e., perpendicular magnetic anisotropy (PMA). In particular, the presence of V_3Ga overall enhances the MAE at the interface due to the strong Fe 3d–V 3d orbital hybridization.[6,31] Notably, a hybrid structure of antiferromagnet–semiconductor/ferromagnet–metal with significant PMA is worthwhile for future research in perpendicular-MTJ-based spintronics devices.[32–35]

3. Conclusion

We have theoretically predicted and experimentally prepared a metastable phase of V_3Ga in the β-W type structure. It was found that such a metastable phase of the sample with good crystallinity can be obtained from alternating evaporation method with post-annealing process, rather than that prepared from the traditional CE method. We have thus experimentally explored a new route to prepare AFM semiconductor materials. The characteristics of magnetic and magnetoresistance properties further revealed that the β-W type V_3Ga exhibits an AFM nature with high Néel temperature in agreement with theoretical prediction. Both experiment and theory have shown that V_3Ga is a highly conductive semiconductor with a narrow bandgap. Moreover, our calculations predicted the large perpendicular magnetic anisotropy at the synthetic V_3Ga/Fe interface, which is attributed to the strong hybridization between the interfacial V d and Fe d orbital states. These features suggest that the β-W type V_3Ga could be a good candidate in an application of AFM spintronics.

4. Experimental Section

Si(001) substrate was first etched in dilute hydrofluoric acid (HF), followed by the desorption of impurities on the substrate surface by heating it to 600 °C for 30 min.[36] Graphite crucibles were used for electron beam evaporation, and tungsten boats were used for thermal evaporation. Elemental metals of Ga and V with purity of 99.99% were used as evaporation materials. There were two preparation procedures used in this experiment. One was via the alternate growth of V and Ga ultrathin multilayers on Si(001) substrate using electron beam evaporation at 450 °C, followed by the postgrowth annealing treatment. Another was via the CE of V and Ga elemental sources simultaneously by electron beam evaporation and thermal evaporation, respectively, at the growth temperature 300 °C. The films with thickness of around 60 nm were prepared under a vacuum of 5×10^{-4} Pa, followed by the growth of a 3 nm Si cap to avoid oxidization of the inner layers of V–Ga. The stoichiometric ratio of V to Ga in the compound was controlled by the evaporation ratio of V and Ga, respectively, which was measured by a quartz thickness monitor. To further confirm the AFM nature of V_3Ga, V_3Ga/Fe bilayer was also prepared. The crystal structure was studied by XRD using Cu Kα radiation. The surface morphology and composition were measured by a field-effect SEM with EDS. Magnetic hysteresis loop was characterized by a vibrating sample magnetometer (VSM). Magnetoresistance and temperature-dependent resistance were measured by a homemade transport property measurement system (TPMS). The temperature-dependent magnetization was characterized using superconducting quantum interference device (SQUID) magnetometry. The bandgap of the sample was determined by UV–vis spectroscopy.

The DFT+U calculations were performed using the projector augmented wave (PAW) pseudopotential method,[37] as implemented in Vienna Ab initio Simulation Package (VASP).[38,39] Exchange and correlation interactions between electrons were described with the generalized gradient approximation (GGA) formulated by Perdew, Burke, and Ernzerhof (PBE).[40] We imposed the Hubbard-type on-site Coulomb energy with $U = 2$ eV and $J = 0.67$ eV parameters onto the V 3d orbitals.[28] We considered two atomic structures, namely $D0_3$, as previous studies addressed[27], and β-W type A15. We also modeled V- and GaV-terminated film slabs consisting of 5–13 atomic layers of V_3Ga films and no less than a 15 Å-thick vacuum region separating the periodic slabs. For bulk and film calculations, we used an energy cutoff of 500 eV and $16 \times 16 \times 16$ and $16 \times 16 \times 1$ Brillouin zone k point meshes for ionic relaxation, respectively, where the forces acting on each atom were less than 10^{-2} eV Å^{-1}. The SOC term is included using the second-variation method, using the scalar-relativistic eigenfunctions of the valence states.[41]

Acknowledgements

This work was supported by the Fundamental Research Funds for the Central Universities (Grant Nos. 2652017344 and 2652017372)and the Basic Science Research Program through the National Research Foundation of Korea (Grant Nos. 2016M3D1A1027831 and 2017R1C1B5017261). N.T. and D.O. acknowledge the support by the National University of Mongolia within the framework of the project P2018-3612.

Conflict of Interest

The authors declare no conflict of interest.

Keywords

V_3Ga, antiferromagnetism, alternating evaporation

Received: August 27, 2019
Published online:

[1] S. Ikeda, K. Miura, H. Yamamoto, K. Mizunuma, H. D. Gan, M. Endo, S. Kanai, J. Hayakawa, F. Matsukura, H. Ohno, *Nat. Mater.* **2010**, *9*, 721.
[2] S. Loth, S. Baumann, C. P. Lutz, D. M. Eigler, A. J. Heinrich, *Science* **2012**, *335*, 196.
[3] X. Marti, I. Fina, C. Frontera, J. Liu, P. Wadley, Q. He, R. J. Paull, J. D. Clarkson, J. Kudrnovsky, I. Turek, J. Kunes, D. Yi, J.-H. Chu, C. T. Nelson, L. You, E. Arenholz, S. Salahuddin, J. Fontcuberta, T. Jungwirth, R. Ramesh, *Nat. Mater.* **2014**, *13*, 367.
[4] R. O. Cherifi, V. Ivanovskaya, L. C. Phillips, A. Zobelli, I. C. Infante, E. Jacquet, V. Garcia, S. Fusil, P. R. Briddon, N. Guiblin, A. Mougin, A. A. Unal, F. Kronast, S. Valencia, B. Dkhil, A. Barthelemy, M. Bibes, *Nat. Mater.* **2014**, *13*, 345.
[5] D. Odkhuu, S. H. Rhim, N. Park, K. Nakamura, S. C. Hong, *Phys. Rev. B* **2015**, *91*, 014437.
[6] D. Odkhuu, *Phys. Rev. B* **2016**, *93*, 064412.
[7] J. Sinova, I. Zutic, *Nat. Mater.* **2012**, *11*, 368.
[8] D. Petti, E. Albisetti, H. Reichlova, J. Gazquez, M. Varela, M. Molina-Ruiz, A. F. Lopeandia, K. Olejnik, V. Novak, I. Fina, B. Dkhil, J. Hayakawa, X. Marti, J. Wunderlich, T. Jungwirth, R. Bertacco, *Appl. Phys. Lett.* **2013**, *102*, 192404.
[9] P. Wadley, B. Howells, J. Zelezny, C. Andrews, V. Hills, R. P. Campion, V. Novak, K. Olejnik, F. Maccherozzi, S. S. Dhesi, S. Y. Martin, T. Wagner, J. Wunderlich, F. Freimuth, Y. Mokrousov, J. Kunes, J. S. Chauhan, M. J. Grzybowski, A. W. Rushforth, K. W. Edmonds, B. L. Gallagher, T. Jungwirth, *Science* **2016**, *351*, 587.

© 2019 WILEY-VCH Verlag GmbH & Co. KGaA, Weinheim

[10] P. Wadley, V. Novak, R. P. Campion, C. Rinaldi, X. Marti, H. Reichlova, J. Zelezny, J. Gazquez, M. A. Roldan, M. Varela, D. Khalyavin, S. Langridge, D. Kriegner, F. Mca, J. Masek, R. Bertacco, V. Holy, A. W. Rushforth, K. W. Edmonds, B. L. Gallagher, C. T. Foxon, J. Wunderlich, T. Jungwirth, *Nat. Commun.* **2013**, *4*, 3322.
[11] P. Wadley, V. Hills, M. R. Shahedkhah, K. W. Edmonds, R. P. Campion, V. Novak, B. Ouladdiaf, D. Khalyavin, S. Langridge, V. Saidl, P. Nemec, A. W. Rushforth, B. L. Gallagher, S. S. Dhesi, F. Maccherozzi, J. Zelezny, T. Jungwirth, *Sci. Rep.* **2015**, *5*, 17079.
[12] H. C. Wu, Z. M. Liao, R. G. S. Sofin, G. Feng, X. M. Ma, A. B. Shick, O. N. Mryasov, I. V. Shvets, *Adv. Mater.* **2012**, *24*, 6374.
[13] V. M. T. S. Barthem, C. V. Colin, H. Mayaffre, M. H. Julien, D. Givord, *Nat. Commun.* **2013**, *4*, 2892.
[14] J. S. Kouvel, C. C. Hartelius, *J. Appl. Phys.* **1962**, *33*, 1343.
[15] S. Maat, J.-U. Thiele, E. E. Fullerton, *Phys. Rev. B* **2005**, *72*, 214432.
[16] C. Stamm, J.-U. Thiele, T. Kachel, I. Radu, P. Ramm, M. Kosuth, J. Minar, H. Ebert, H. A. Durr, W. Eberhardt, C. H. Back, *Phys. Rev. B* **2008**, *77*, 184401.
[17] I. Suzuki, M. Itoh, T. Taniyama, *Appl. Phys. Lett.* **2014**, *104*, 022401.
[18] D. Odkhuu, *Phys. Rev. B* **2017**, *96*, 134402.
[19] C. Bordel, J. Juraszek, D. W. Cooke, C. Baldasseroni, S. Mankovsky, J. Minar, H. Ebert, S. Moyerman, E. E. Fullerton, F. Hellman, *Phys. Rev. Lett.* **2012**, *109*, 117201.
[20] I. Galanakis, P. H. Dederichs, N. Papanikolaou, *Phys. Rev. B* **2002**, *66*, 174429.
[21] C. Felser, G. H. Fecher, B. Balke, *Angew. Chem. Int. Ed.* **2007**, *46*, 668.
[22] T. Graf, C. Felser, S. S. P. Parkin, *Prog. Solid State Chem.* **2011**, *39*, 1.
[23] S. Skaftouros, K. Ozdogan, S. S. P. Sasioglu, I. Galanakis, *Phys. Rev. B* **2013**, *87*, 024420.
[24] X. L. Wang, *Phys. Rev. Lett.* **2008**, *100*, 156404.
[25] S. Skaftouros, K. Ozdogan, E. Sasoglu, I. Galanakis, *Appl. Phys. Lett.* **2013**, *102*, 022402.
[26] M. E. Jamer, B. A. Assaf, G. E. Sterbinsky, D. Arena, L. H. Lewis, A. A. Saul, G. Radtke, D. Heiman, *Phys. Rev. B* **2015**, *91*, 094409.
[27] I. Galanakis, S. Tirpanci, K. Ozdogan, E. Sasioglu, *Phys. Rev. B* **2016**, *94*, 064401.
[28] T. Berlijn, P. C. Snijders, O. Delaire, H.-D. Zhou, T. A. Maier, H.-B. Cao, S.-X. Chi, M. Matsuda, Y. Wang, M. R. Koehler, P. R. C. Kent, H. H. Weitering, *Phys. Rev. Lett.* **2017**, *118*, 077201.
[29] H. Danan, A. Herr, A. J. P. Meyer, *J. Appl. Phys.* **1968**, *39*, 669.
[30] S. Ramakrishnan, A. K. Nigam, G. Chandra, *Phys. Rev. B* **1986**, *34*, 6166.
[31] D. Odkhuu, S. H. Rhim, N. Park, S. C. Hong, *Phys. Rev. B* **2013**, *88*, 184405.
[32] D. Odkhuu, *Phys. Rev. B* **2017**, *96*, 134402.
[33] D. Odkhuu, *Sci. Rep.* **2018**, *8*, 6900.
[34] D. Odkhuu, *J. Magn. Magn. Mater.* **2019**, *476*, 487.
[35] D. Odkhuu, *IEEE Trans. Magn.* **2019**, *55*, 7000104.
[36] W. Feng, D. D. Dung, Y. Shin, D. V. Thiet, S. Cho, X. Hao, *J. Kor. Phys. Soc.* **2010**, *56*, 1382.
[37] P. E. Blöchl, *Phys. Rev. B* **1994**, *50*, 17953.
[38] G. Kresse, J. Hafner, *Phys. Rev. B* **1993**, *47*, 558(R).
[39] G. Kresse, J. Furthmüller, *Phys. Rev. B* **1996**, *54*, 11169.
[40] J. P. Perdew, K. Burke, M. Ernzerhof, *Phys. Rev. Lett.* **1996**, *77*, 3865.
[41] D. D. Koelling, B. N. Harmon, *J. Phys. C* **1977**, *10*, 3107.

© 2019 WILEY-VCH Verlag GmbH & Co. KGaA, Weinheim